Published in final edited form as:
J Phys Chem B. 2009 January 15; 113(2): 522–530. doi:10.1021/jp806727e.

Synchronous vs. Asynchronous Chain Motion in α-Synuclein Contact Dynamics

Kristopher G. Urie[†], **David Angulo**[†], **Jennifer C. Lee**[‡], **John J. Kozak**[*,†], **Harry B. Gray**[*,§], and **Jay R. Winkler**[*,§]
Department of Chemistry, DePaul University, Chicago, Illinois, 60604-2301, Laboratory of Molecular Biophysics, National Heart, Lung, and Blood Institute, National Institutes of Health, Bethesda, Maryland 20892-8013, Beckman Institute, California Institute of Technology, Pasadena, California 91125-7400

Abstract

α-Synuclein (α-syn) is an intrinsically unstructured 140-residue neuronal protein of uncertain function that is implicated in the etiology of Parkinson's disease. Tertiary contact formation rate constants in α-syn, determined from diffusion-limited electron-transfer kinetics measurements, are poorly approximated by simple random polymer theory. One source of the discrepancy between theory and experiment may be that interior-loop formation rates are not well approximated by end-to-end contact dynamics models. We have addressed this issue with Monte Carlo simulations to model asynchronous and synchronous motion of contacting sites in a random polymer. These simulations suggest that a dynamical drag effect may slow interior loop formations rates by about a factor of two in comparison to end-to-end loops of comparable size. The additional deviations from random coil behavior in α-syn likely arise from clustering of hydrophobic residues in the disordered polypeptide.

Keywords

electron transfer; Parkinson's disease; Monte Carlo simulations

1. Introduction

A well-defined three-dimensional structure (fold) is a property commonly attributed to native proteins. Yet, the more than 1000 unstructured regions that have been identified in over 400 different polypeptides reveal that disorder is a defining characteristic of a great many natural biopolymers.[1] These disordered polypeptides are believed to play important functional roles[2] that will depend in no small part on their conformational dynamics.

We have exploited the excited-state properties of tryptophan residues to probe structural preferences and conformational dynamics in α-synuclein (α-syn), an intrinsically unstructured 140-residue neuronal protein of uncertain function that is implicated in the etiology of Parkinson's disease.[3] In particular, tertiary contact formation rate constants in α-syn have been determined from kinetics measurements of diffusion-limited electron-transfer between triplet-excited tryptophan (^{3}W*, donor) and 3-nitrotyrosine (acceptor) groups separated by n = 10,

*Corresponding author. E-mail: kozak@depaul.edu (J.J.K.); hbgray@caltech.edu (H.B.G); winklerj@caltech.edu (J.R.W.).
[†]DePaul University, 243 South Wabash Ave, Chicago, IL 60604-2301
[‡]National Heart, Lung, and Blood Institute
[§]Beckman Institute

12, 15, 20, 35, 42, 55, 90 and 132 residues (Figure 1).[4,5] Continuum models for random polymers predict that end-to-end contact rates will exhibit a power-law dependence on *n*, the number of links in the polymer chain.[6] The magnitude of the scaling exponent depends somewhat on solvent conditions, but typically falls in the range −1.5 to −1.8.[6–8] The α-syn tertiary contacts rates, however, are poorly approximated by a $n^{-1.5}$ function (Figure 1); the deviations from power-law behavior suggest that although the polypeptide is disordered, it is not a random polymer.[4,9]

The energy landscapes for intrinsically unstructured proteins are unlikely to be smooth flat surfaces, hence simple random coil behavior is not expected.[2] Nevertheless, this simple polymer model is a natural starting point for comparison to α-syn properties. In prior work, we developed a Markovian lattice model to describe intrachain diffusion dynamics for a disordered polypeptide;[5] when employed to predict α-syn contact quenching rates, reasonable agreement with the experimentally determined values for small loops (10-20 residues) was obtained, but important qualitative differences emerged with further increases in loop size ($n > 35$ residues). Whereas the (numerically exact) results obtained in solving the Markovian model were instructive, one or more of the assumptions introduced in formulating the model restricted its usefulness.

The diffusion coefficient (*D*) extracted from the experimental data exhibits a systematic increase with *n*.[4] It was suggested there that the "dependence of *D* on *n* may be a reflection of greater chain stiffness in the smaller loops." It was also noted that another factor affecting the values of *D* could be the hydrodynamic drag of the polypeptide external to the tertiary contact loop.[10]

With respect to the first of these possibilities, the role of chain stiffness in influencing the magnitude of the rate constant was taken into account by studying the exact Markovian dynamics on lattices of cubic and tetrahedral symmetries.[5,11] Using random-walk data derived from our Markovian analysis in concert with Domb's seminal results on self-avoiding walks, [12] a correlation with an expression derived by Hyeon and Thirumalai[13] for contact rates was developed. Although the quantitative agreement between these two approaches was modest, both predict a steeper decrease in contact rate with increasing *n* for the simple cubic lattice than for the tetrahedral one, a consequence of the fact that on the former lattice a diffusing species has two additional (motional) degrees of freedom at each vertex site. The faster growth in configurational entropy as polymer size increases is responsible for a steeper decay in contact rate constants for more flexible polymers.[5]

With respect to the second of the two factors cited above, a possible drag effect arising from regions of the polypeptide chain external to the contact loop was not considered in our prior calculations.[5] Rather, it was assumed that one member of the donor/acceptor pair was anchored at one vertex of the host lattice, with the other moiety free to diffuse (subject to the topology of the lattice). The advantage of this formulation was that one could extract from the numerically exact results (on the mean walklength before contact) analytical expressions that could be used to predict the rate constants for large loop sizes. The disadvantage was that effects arising from restricted diffusional motion of both donor and acceptor, owing to the (two) polypeptide chains external to the contact loop, were neglected and no assessment of their importance was made.

In this study we generalize our prior stochastic lattice model to examine the possible influence of drag on contact quenching rates.[5] In order to account for this effect, we must address the problem of asynchronous versus synchronous motion of donor and acceptor on the efficiency of contact formation probed by diffusive electron transfer. The price for expanding the generality of the model along these lines is that we must resort to numerical methods, here

Monte Carlo simulations, to quantify effects. However, the reliability of the results obtained can be gauged by comparison with the numerically exact results on the restricted model studied earlier for asynchronous motion,[5] and with both analytical and numerical results reported in an extensive study of synchronous Markovian dynamics.[14]

2. Methods

Modeling Asynchronous and Synchronous Chain Motion

To explore quantitatively the possibility that the dependence of the diffusion coefficient D on the loop size n is attributable to drag of the polypeptide chain external to the tertiary contact loop, several interrelated assumptions in our Markov model must be relaxed. First, we lift the restriction[5] that the maximum volume accessible to a diffusing moiety is the volume enclosed by a loop of length n. We now consider the volume swept out by a radial vector whose magnitude is the length of the fully extended polypeptide chain linking donor and acceptor. This generalization captures the full phase space available to diffusing species, thus allowing a more accurate portrayal of the configurational entropy.

Second, we relax the constraint that one member of the donor/acceptor pair is stationary, and explore the consequences of assuming that both species can diffuse simultaneously in configurational space. If we denote by $N(\mathrm{D})$ the number of residues from the terminal end of the polypeptide chain to the donor site, and by $N(\mathrm{A})$ the number of residues from the (other) terminal end to the acceptor site, then when $N(\mathrm{A}) \gg N(\mathrm{D})$ we assume that the donor will diffuse asynchronously with respect to the acceptor [or, vice versa when $N(\mathrm{D}) \gg N(\mathrm{A})$]. However, when $N(\mathrm{A}) \sim N(\mathrm{D})$, it is more likely that the dynamics characterizing the mutual displacements and eventual encounter of donor and acceptor will have more synchronous character.

To characterize and discriminate among degrees of synchronicity, we use a physical metric based on the masses of the polypeptides external to the D/A loop. We compute (in Daltons) the net masses ($M(\mathrm{A})$, $M(\mathrm{D})$) corresponding to the sequence of residues, $N(\mathrm{A})$ and $N(\mathrm{D})$, respectively. Then, as our synchronicity metric, we construct a mass ratio R such that R is (always) bounded between zero and one [viz., $R = M(\mathrm{A})/M(\mathrm{D})$ if $M(\mathrm{A}) < M(\mathrm{D})$, and vice versa] (Eq. 1). Values of R approaching zero, then, correspond to the

$$0 \leq R \leq 1 \tag{1}$$

asynchronous limit, and values $R \rightarrow 1$ to the limiting case of totally synchronous displacements of donor and acceptor.

Each trial in the Monte Carlo simulation consisted of three phases: initialization, walk, and termination. At initialization, the acceptor particle was placed at the origin of the lattice, while the donor particle was given a random position on the lattice. During the trial, each particle was given some constant probability of moving during a time step. For example, in the totally asynchronous case, $p(\mathrm{D}) = 1$ and $p(\mathrm{A}) = 0$ (or vice versa). In the totally synchronous case, $p(\mathrm{D}) = p(\mathrm{A}) = 1$. A move consists of a unit step in any randomly chosen direction allowed by the lattice, subject to some boundary condition. Three-dimensional simulations included walks on both cubic and tetrahedral lattices. On a cubic lattice, six different moves are allowed from each position in the lattice, while on a tetrahedral lattice, four different moves are allowed.

The physically relevant boundary condition for the confining case was the passive boundary, in which a donor (or acceptor) that attempts to move outside the lattice was reset to its previous position. A different constraint was imposed in the extended chain case: donor and acceptor were reset to prior positions if they attempted a move that would separate them beyond the

chain length. Thus, in the totally asynchronous, extended chain case, the donor (acceptor) is restricted to a spherical region around the (stationary) acceptor (donor). Similarly, in the synchronous case, each particle is restricted to a spherical region around the other, but the possible locations of the pair on the lattice are effectively unbounded.

Trials were terminated by contact between the donor and acceptor particles. Contact could be achieved in either of two ways: superposition or position swap. If, at the end of a time step, the two particles were in the same position, the walk was terminated. Alternatively, if the particles were each at the other's previous position, they were judged to have achieved contact during the time step (at $t+ ½$) and the walk was terminated.

Consider first the asynchronous case. The quality of the simulations can be gauged via comparison with earlier Monte Carlo results or with numerically exact results obtained via the theory of finite Markov processes.[11] One acid test is to consider a particle undergoing an unbiased random walk on a one-dimensional ($d = 1$) lattice of N sites subject to periodic boundary conditions, and to calculate the mean number $\langle x \rangle$ of displacements (mean walklength) before localization (trapping) of the random walker. Montroll obtained an exact analytical expression for this case in the form of Eq. 2:[15–17]

$$\langle x \rangle = \frac{N(N+1)}{6} \tag{2}$$

As may be seen from Table 1, results obtained via our Monte Carlo simulations are in excellent agreement with values calculated using Montroll's formula.

Similarly, for the synchronous case, we consider two random walkers undergoing simultaneous random displacements on a $d = 1$ lattice of N sites subject to periodic boundary conditions, and calculate the mean number of displacements before a first encounter of the two walkers. In this case, exact analytical expressions have been obtained;[18] the calculated results (Eqs. 3a, 3b) and the Monte Carlo simulations are in excellent agreement (Table 1).

$$\langle x \rangle = \frac{N(N+1)(N+2)}{12(N-1)} \quad (N \text{ even}) \tag{3a}$$

$$\langle x \rangle = \frac{(N+1)(N+3)}{12} \quad (N \text{ odd}) \tag{3b}$$

Set out in Tables 2–3 are the results for the mean number $\langle x \rangle$ of displacements before donor-acceptor contact on a ($d = 3$ dimensional) simple cubic lattice. In the previous model,[5] we identified the (maximum) lattice volume encompassed by a given setting of n, the number of residues separating donor and acceptor. For the asynchronous case, the results obtained via Monte Carlo simulation can be compared with the numerically exact Markov results,[5] and the agreement is found to be excellent (Table 2). No analytical results are available for the case of (totally) synchronous motion of donor and acceptor, but the 95% confidence interval of the mean is a measure of the quality of the simulations. The mean walklengths for the asynchronous case increased from 1.6 to 2.7 times longer than the corresponding walklengths using the synchronous model as the chain length increased.

The data reported in Table 3 explore the consequences of considering the volume swept out by a radial vector whose magnitude is the length of the fully extended polypeptide chain linking the donor and acceptor. Notice that the walks for this case (extended chain) are much larger than those calculated for the maximum loop, a point to which we shall return. In the extended-chain case, the simulations were run until the confidence interval calculated (based on the mean and the number of trials) was less than 5% of the current mean; to avoid a spurious termination, owing to a few lucky initial trials, (at least) 1000 trials were made before the interval was calculated. The ratio of aynchronous-to-synchronous walklengths for the extended volume model was a relatively constant 1.2. It appears that when the full volume of the extended polymer is considered, the differential effects of synchronous and asynchronous motion are reduced.

Plots of the mean displacement $\langle x \rangle$ on 9×9×9 and 10×10×10 cubic lattices as a function of the synchronous-motion probability (p) over the full range ($0 \leq p \leq 1$) are shown in Figure 2. Notice that results displayed are for three choices of the boundary condition imposed on the donor/acceptor upon confronting the surface of the enclosed volume. The physically relevant boundary condition (labeled passive) corresponds to the case in which the donor or acceptor is simply reset at that boundary site when it attempts to step out of the lattice. For comparison, the results for reflective boundary conditions (the donor/acceptor is reset at a nearest-neighbor site interior to the volume) and periodic boundary conditions (the donor/acceptor is reset at a site symmetrically disposed on the opposite side of the lattice) are given. For both the maximum loop case[5] and the extended chain case, we may conclude from the results summarized in Tables 2–3 and Figure 2 that synchronous motion of donor and acceptor leads to more efficient contact quenching than for the case when one or other of the partners is localized.

In our earlier study, the consequences of chain stiffness were explored by comparing the mean displacements $\langle x \rangle$ calculated for the asynchronous case on cubic versus tetrahedral lattices (see earlier discussion).[5] The profiles displayed in Figure 3 for asynchronous and synchronous motion illustrate the behavior of $\langle x \rangle$ as a function of the total number of lattice sites (N), computed for cubic versus tetrahedral lattices, and for passive boundary conditions. Then, in Figure 4, results are shown for $\langle x \rangle$ versus the probability of synchronous motion (p) on a lattice of $N = 1000$ sites, again for passive boundary conditions.

Recalling that the contact rate constant k is inversely proportional to $\langle x \rangle$,[5] the results presented in Figures 3 and 4 show convincingly that rate processes on tetrahedral lattices of N total sites are slower than those on corresponding cubic ones. The influence on the kinetics of chain stiffness is in this case a direct consequence of there being two fewer degrees of freedom available to a diffusing donor/acceptor on a tetrahedral lattice.

3. Comparison of Simulation and Experimental Results

Similarities and differences in the net masses of the two terminal polypeptide chains necessarily influence the dynamics of chain motion and loop closure. A significant disparity in the mass of the two chains will confer asynchronicity on the relative motion of donor and acceptor. However, as the mass of each chain approaches parity, the relative motion of donor and acceptor should be characterized by more synchronous displacements.

The principal conclusion following from the Monte Carlo simulations on synchronous vs. asynchronous motion of donor and acceptor is that contact quenching is more efficient when both are moving simultaneously. That is, all other things being equal, the rate constant for synchronous motion should be greater than for asynchronous motion. Contact rate constants will be proportional to the reciprocals of the mean walklengths so, by introducing a suitable

proportionality constant (10^8 in this case), we can compare the results of our lattice model simulations to the experimental contact rate data (Figure 5).

It is worth noting that the profiles displayed in Figure 5 for asynchronous and synchronous motion both exhibit a crossover with respect to the underlying lattice topology, cubic vs. tetrahedral. This crossover was noted previously for asynchronous motion.[5] Here, we find that introducing synchronicity has the consequence of displacing the crossover to much shorter contact loop sizes. Inasmuch as differences in chain stiffness can be gauged by studies on lattices of different topology, the consequences of introducing synchronicity on the contact rate constants for small versus large contact loops may well be significant (*vide infra*).

For a given position of donor and acceptor on α-syn, there will be residues on the N-terminal side of one partner and a (different) number of residues on the C-terminal side of the other partner. As noted above, we use the accepted mass (in Daltons) of each amino acid to quantify the (net) mass of the polypeptide chains external to the segment between donor-acceptor pair, and then construct the ratio, *R*.

Consider now the experimental data on contact quenching rates and the synchronicity metric (the ratio *R*) for Trp-containing (W site) and Tyr(NO_2)-containing (Y site) α-syn mutants (Table 4).[4,5] With the W4 donor, average contact rate constants tend to decrease with increasing loop size, although there is approximately a twofold *increase* in contact rate on going from $n = 90$ to 132. Noting that the values of *R* for the $n \leq 90$ cases are in the asynchronous range, the trend observed is entirely consistent with the Markovian analysis and results that predicted (quantitatively) a systematic decrease in rate constant with increasing loop size *n*.[4] The drift upward in magnitude of the rate constant for $n = 132$ may be rationalized by noting that the value of the ratio *R* falls in the range $R \rightarrow 1$. The behavior in this regime is expected to be qualitatively different. The Monte Carlo data show clearly that, relative to the asynchronous case, the synchronous diffusion of donor and acceptor should result in a larger rate constant.

The two contact rate constants determined for $n = 20$ loops are virtually identical, although they have substantially different values of *R* (Table 4). The mass ratio for the W94/Y(NO_2)74 loop suggests that its motion would be better represented by the synchronous limit than that of the W39/Y(NO_2)19 loop. The diffusion coefficients (*D*) extracted from analyses of energy- and electron-transfer quenching in the two proteins are consistent with this prediction (W94/Y(NO_2)74, $D = 3.2 \times 10^{-6}$ cm^2 s^{-1}; W39/Y(NO_2)19, $D = 1.7 \times 10^{-6}$ cm^2 s^{-1}). That the contact rates do not reflect this trend is likely a consequence of nonrandom structure in these regions of the α-syn polypeptide.

Finally, we consider three cases where the W site is fixed at residue 94 (Table 4). The contact rate constants for $n = 20$ and 42 loops are quite close and that for the $n = 55$ loop is about 30% smaller. In these cases, neither the rate constants nor diffusion coefficients reflect the predicted effects of synchronous and asynchronous motion. Again nonrandom structure of the polypeptide is the likely explanation (*vide infra*).

4. Concluding Remarks

Tertiary contact dynamics in disordered peptides and proteins have been the subject of extensive experimental and theoretical investigations.[7,8,10,13,19–26] The contact rate constants in α-syn, particularly for $n \leq 30$, are substantially smaller (up to 100 fold) than those reported for D-(Gly-Ser)$_m$-A peptides of comparable loop sizes.[7] An important distinction between the two sets of experiments is that internal loops are being formed in α-syn, whereas end-to-end contacts are formed in D-(Gly-Ser)$_m$-A peptides. Theoretical analyses of internal loop formation that address the effects of chain stiffness[13] and excluded volume[26] suggest that, at comparable values of *n*, internal loop formation rates will be 2 to 4 times smaller than end-to-

end contact rates. These results parallel those found for the ratio of asynchronous to synchronous mean walklengths on cubic and tetrahedral lattices. Hence, some combination of chain stiffness, excluded volume effects, and dynamical drag likely can account for up to one order of magnitude reduction in contact rates for interior loops.[10]

Thirumalai has suggested that contact rate constants in semiflexible polymers depend on an effective monomer diffusion coefficient (D_o), the mean squared distance between the contacting residues ($<r^2>$), and the probability of loop formation ($P(n)$) (Eq. 4).[13,25]

$$k_T \approx \frac{D_o P(n)}{\left\langle r_n^2 \right\rangle} \tag{4}$$

In a study of excluded volume effects for two- and three-dimensional lattices, Domb demonstrated that $<r^2> \sim n^{6/5}$ for both cubic and tetrahedral lattices.[12] Loop formation probabilities for the two lattices vary approximately as $P(n) \sim n^{-3.3}$ (cubic) and $P(n) \sim n^{-2.6}$ (tetrahedral) (see Appendix).[5] Hence, lattice model predictions for the dependence of specific contact rates on loop size are $k_T \sim n^{-2.1}$ (cubic) and $k_T \sim n^{-1.4}$ (tetrahedral). Within the context of Thirumalai's model, anomalous values of the diffusion coefficient, the average distance between the contacting residues, and/or the loop formation probability must be responsible for the discrepancies between α-syn and synthetic peptide tertiary contact dynamics.

The diffusion coefficient extracted from an analysis of fluorescence energy transfer kinetics in D-(Gly-Ser)$_m$-A (4.9×10^{-6} cm^2 s^{-1})[24,27] is on par with those found in global analyses of W*→ Y(NO$_2$) energy- and electron-transfer kinetics in α-syn ($1 - 6 \times 10^{-6}$ cm^2 s^{-1}).[4] The modest differences in D_o are consistent with the magnitude of the drag effect estimated in the Markov model simulations. The Stokes-Einstein equation predicts that the diffusion coefficient for a large particle moving through a fluid continuum is inversely proportional to the radius of the particle. Introduction of peptide residues external to the loop might be expected to increase the effective particle radius and reduce the diffusion coefficient. Yet, Kiefhaber's observation that the dependence of internal loop formation rates on solvent viscosity does not vary with the length of the external tail in synthetic peptides[10] points to a minor role for hydrodynamic drag. Hence, differences in effective diffusion coefficients arising from internal versus external loop formation only account for part of the deviation of α-syn tertiary contact rates from the predictions of random polymer theory.

NMR spin-label experiments on α-syn and molecular dynamics simulations suggest that the protein is "significantly more compact than a random coil," and that "this partial condensation is driven by long-range contacts between residues 120-140 in the negatively charged C-terminal tail and residues 30-100 in the center of the protein".[9] Moreover, Gaussian chain distance distributions poorly represent ^{1}W*→Y(NO$_2$) fluorescence energy-transfer kinetics in α-syn and, in contrast to the behavior of D-(Gly-Ser)$_m$-A peptides, the ^{3}W*→Y(NO$_2$) contact quenching kinetics are decidedly nonexponential. These data provide clear evidence for preferred conformations in the energy landscape of the protein that will produce significant deviations in $<r^2>$ and $P(n)$ from the values expected for random polymers.

Deviations from random coil behavior in α-syn could arise from clustering of hydrophobic residues. Hydrophobicity scales typically are based on free energies of transfer of amino acid side chains from water to apolar environments (*e.g.*, organic solvents, gas phase).[28] Regardless of the details of the scale used, amino acids with aliphatic side chains (L, I, V, A) are the most hydrophobic of the twenty naturally occurring residues and, hence, most likely to form clusters when the polypeptide is disordered. A rendering of the α-syn polypeptide in which the amino

acid side chains are colored according to a coarse hydophobicity scale[29] reveals several large segments containing L, I, V, and A (Figure 6). It is likely that clustering of residues in these regions are responsible for the significant departures of α-syn contact dynamics from behavior expected for random polymers.

Acknowledgments

This research was supported by grants from the National Institutes of Health (GM068461 to JRW; DK19038 to HBG) and the Ellison Medical Foundation (Senior Scholar Award in Aging to HBG), and by the Intramural Research Program of the National Institutes of Health, the National Heart, Lung, and Blood Institute (JCL).

References

1. Sickmeier M, Hamilton JA, LeGall T, Vacic V, Cortese MS, Tantos A, Szabo B, Tompa P, Chen J, Uversky VN, Obradovic Z, Dunker AK. Nucl Acids Res 2007;35:D786–D793. [PubMed: 17145717]
2. Dyson HJ, Wright PE. Nature Rev Molec Cell Biol 2005;6:197–208. [PubMed: 15738986]
3. Wenning GK, Jellinger KA. Curr Opin Neurol 2005;18:357–362. [PubMed: 16003109]
4. Lee JC, Gray HB, Winkler JR. J Am Chem Soc 2005;127:16388–16389. [PubMed: 16305213]
5. Lee JC, Lai BT, Kozak JJ, Gray HB, Winkler JR. J Phys Chem B 2007;111:2107–2112. [PubMed: 17279794]
6. Szabo A, Schulten K, Schulten Z. J Chem Phys 1980;72:4350–4357.
7. Krieger F, Fierz B, Bieri O, Drewello M, Kiefhaber T. J Mol Biol 2003;332:265–274. [PubMed: 12946363]
8. Lapidus LJ, Eaton WA, Hofrichter J. Proc Natl Acad Sci USA 2000;97:7220–7225. [PubMed: 10860987]
9. Dedmon MM, Lindorff-Larsen K, Christodoulou J, Vendruscolo M, Dobson CM. J Am Chem Soc 2005;127:476–477. [PubMed: 15643843]
10. Fierz B, Kiefhaber T. J Am Chem Soc 2007;129:672–679. [PubMed: 17227031]
11. Kozak JJ. Adv Chem Phys 2000;115:245–406.
12. Domb C. J Chem Phys 1963;38:2957–2963.
13. Hyeon C, Thirumalai D. J Chem Phys 2006;124:104905. [PubMed: 16542102]
14. Abad E, Kozak JJ. Physica A 2006;370:501–524.
15. Montroll EW. Proc Symp Appl Math 1963;16:193–220.
16. Montroll EW, Weiss GH. J Math Phys 1965;6:167–181.
17. Montroll EW. J Math Phys 1969;10:753.
18. Bentz JL, Kozak JJ, Abad E, Nicolis G. Physica A 2003;326:55–68.
19. Hagen SJ, Hofrichter J, Eaton WA. J Phys Chem B 1997;101:2352–2365.
20. Hagen SJ, Hofrichter J, Szabo A, Eaton WA. Proc Natl Acad Sci USA 1996;93:11615–11617. [PubMed: 8876184]
21. Lapidus LJ, Eaton WA, Hofrichter J. Phys Rev Lett 2001;87258101-258101-258101-258104
22. Kubelka J, Hofrichter J, Eaton WA. Curr Opin Struct Biol 2004;14:76–88. [PubMed: 15102453]
23. Bieri O, Wirz J, Hellrung B, Schutkowski M, Drewello M, Kiefhaber T. Proc Natl Acad Sci USA 1999;96:9597–9601. [PubMed: 10449738]
24. Moglich A, Joder K, Kiefhaber T. Proc Natl Acad Sci USA 2006;103:12394–12399. [PubMed: 16894178]
25. Thirumalai D. J Phys Chem B 1999;103:608–610.
26. Doucet D, Roitberg A, Hagen SJ. Biophys J 2007;92:2281–2289. [PubMed: 17208979]
27. Moglich A, Joder K, Kiefhaber T. Proc Natl Acad Sci USA 2008;105:6787.
28. Karplus PA. Prot Sci 1997;6:1302–1307.
29. Wolfenden R, Andersson L, Cullis PM, Southgate CCB. Biochemistry 1981;20:849–855. [PubMed: 7213619]
30. Ulmer TS, Bax A, Cole NB, Nussbaum RL. J Biol Chem 2005;280:9595–9603. [PubMed: 15615727]

Appendix

Appendix

In our prior study,[5] the probability of loop formation, $P(n)$ was approximated by the reciprocal of the number of lattice sites (N); a least-squares fit to a power dependence yielded expressions A1a and A1b for cubic and tetrahedral lattices, respectively.

$$P(n)=n^{-3.3} \quad \text{(cubic)} \tag{A1a}$$

$$P(n)=n^{-2.6} \quad \text{(tetrahedral)} \tag{A1b}$$

We have now developed *analytical* expressions for $P(n)$ for simple cubic and tetrahedral lattices. If n is the maximum (surface) loop, then it can be shown that expressions A2a and A2b describe cubic and tetrahedral lattices, respectively. Values of $P(n)$ calculated using A1 and A2 differ by a factor of ten for small loop sizes, but the values converge (and eventually intersect) with increase in n.

$$P(n)=(n/6+1)^{-3} \text{ (cubic)} \tag{A2a}$$

$$P(n)=[([n/6+1]+1)([n/6+1]+2)(2\times[n/6+1]+3)/6]^{-1} \text{ (tetrahedral)} \tag{A2b}$$

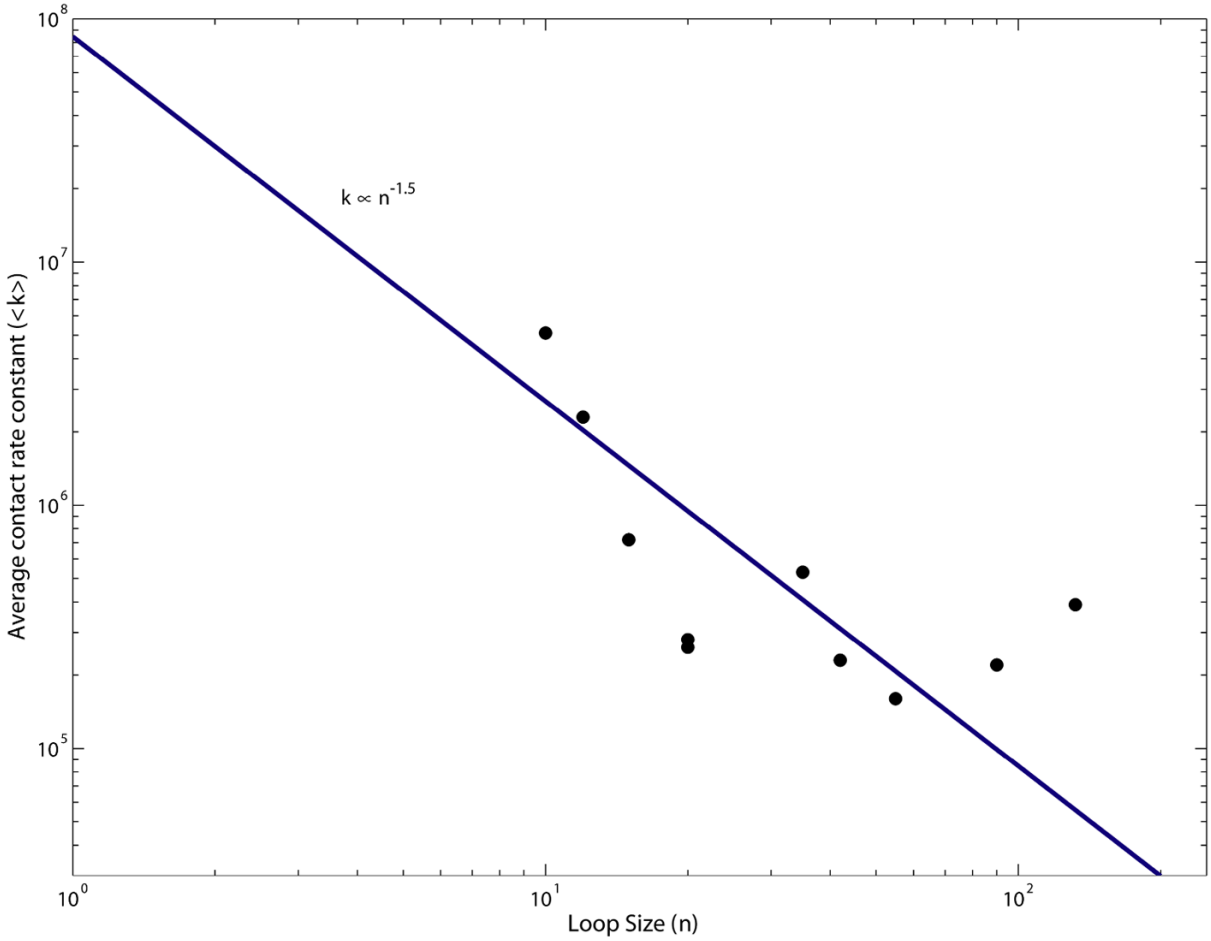

Figure 1.

Dependence of average α-syn contact rate constants on the number of residues (*n*) separating the electron donor (W) and acceptor (Y(NO_2)). Solid line is best fit to a $k \sim n^{-1.5}$ power law dependence.

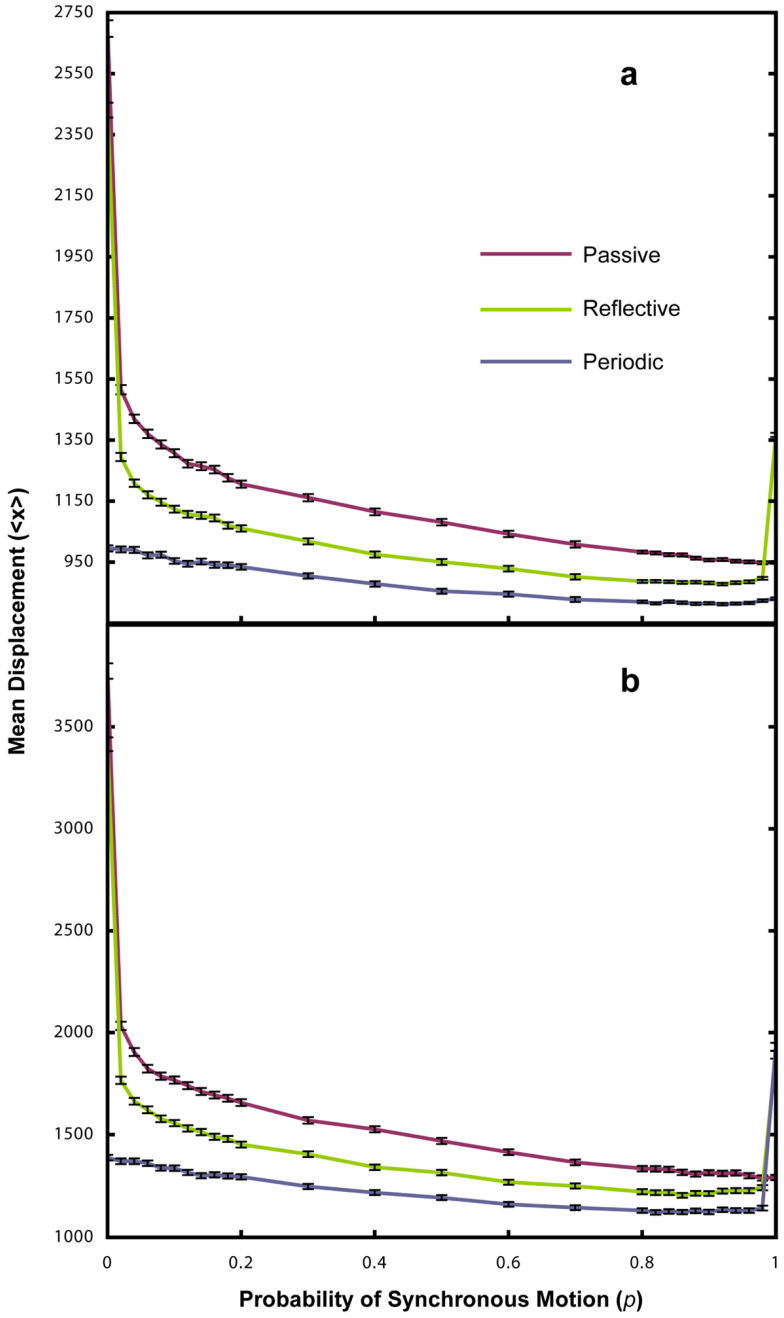

Figure 2.
Mean displacements $\langle x \rangle$ as functions of the probability of synchronous motions (p) on odd-numbered (9×9×9) (**a**) and even-numbered (10×10×10) (**b**) cubic lattices with passive (red), reflective (green), and periodic (blue) boundary conditions.

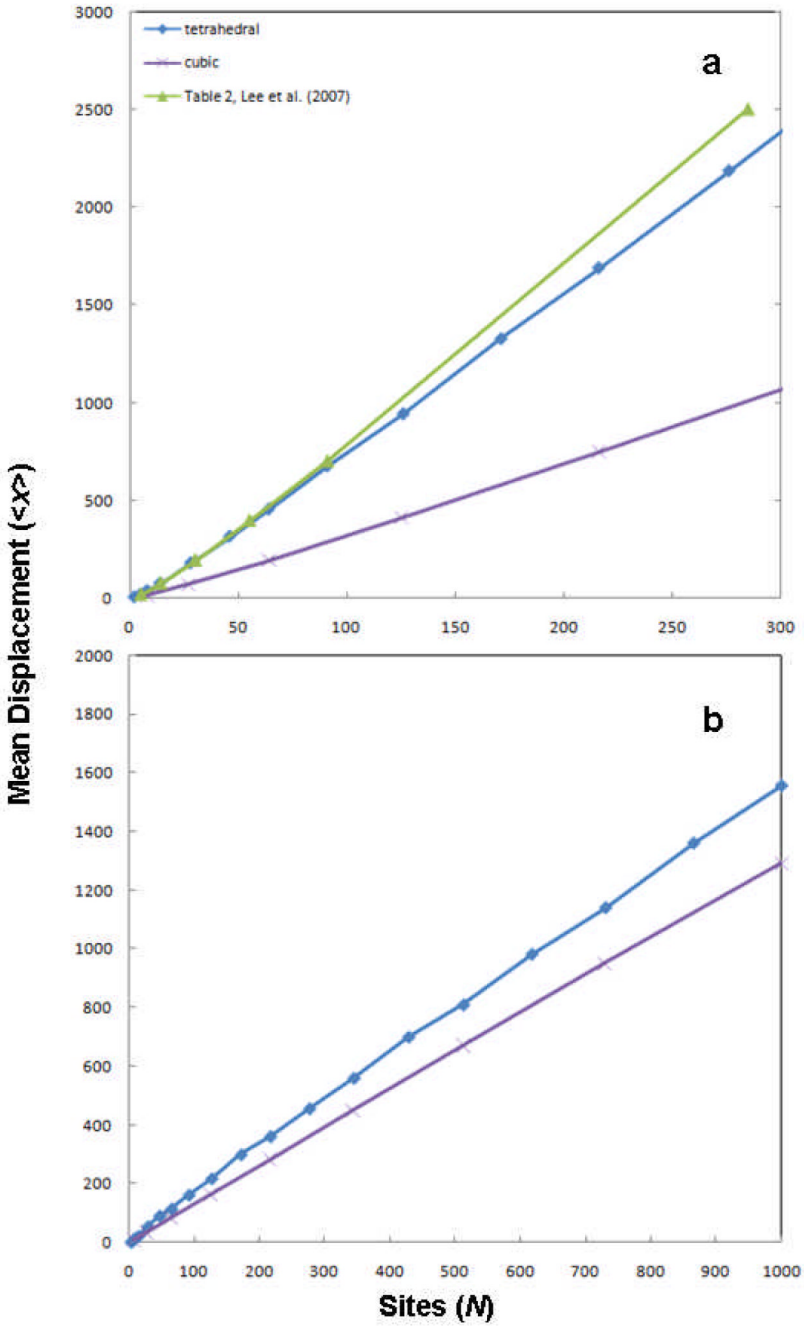

Figure 3.

(a) The growth of mean displacement with lattice size for asynchronous motion ($p = 0$) on cubic and tetrahedral lattices, with a comparison to the results of Ref. 5. (b) The growth of mean displacement with lattice size for synchronous motion ($p = 1$) on cubic and tetrahedral lattices.

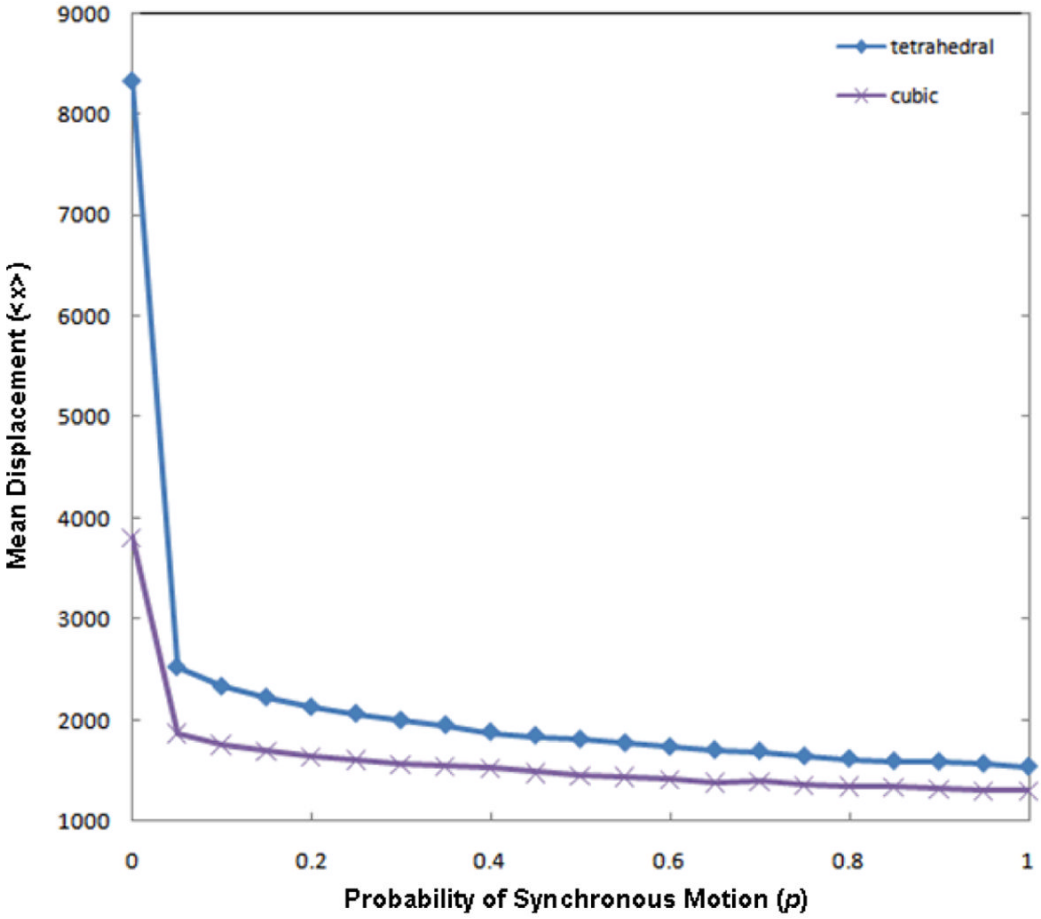

Figure 4.
Mean displacement on 1000-site cubic and tetrahedral lattices with confining boundary conditions.

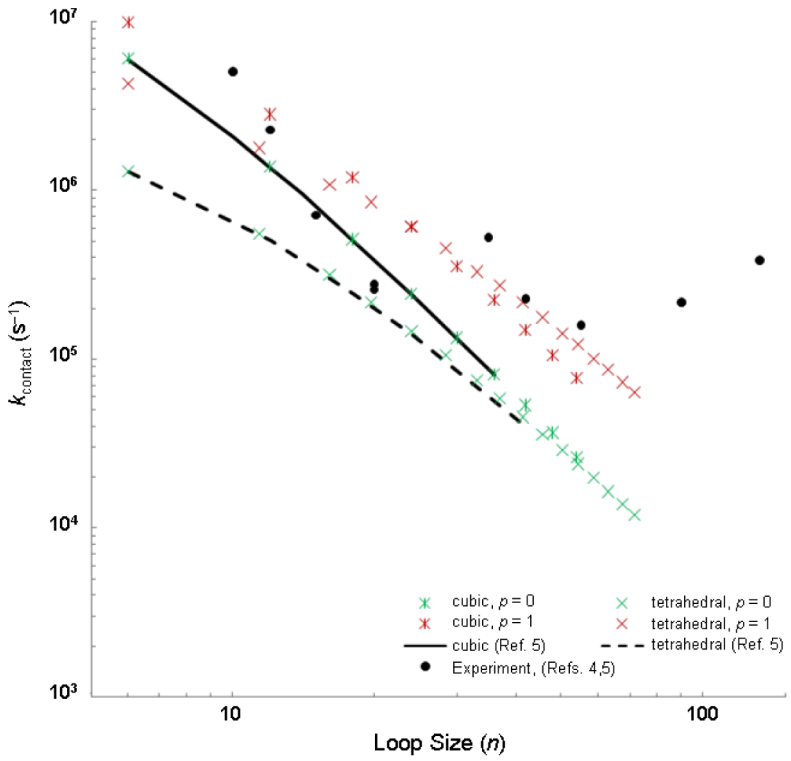

Figure 5.

Rate constants (inverse mean walklengths scaled by 10^8 s^{-1}) calculated for asynchronous ($p = 0$) and synchronous ($p = 1$) motion with maximum-loop (solid and dashed lines, Ref. 5) and extended-chain constraints (×,(). Experimental α-syn contact rate constants are shown as solid black circles.

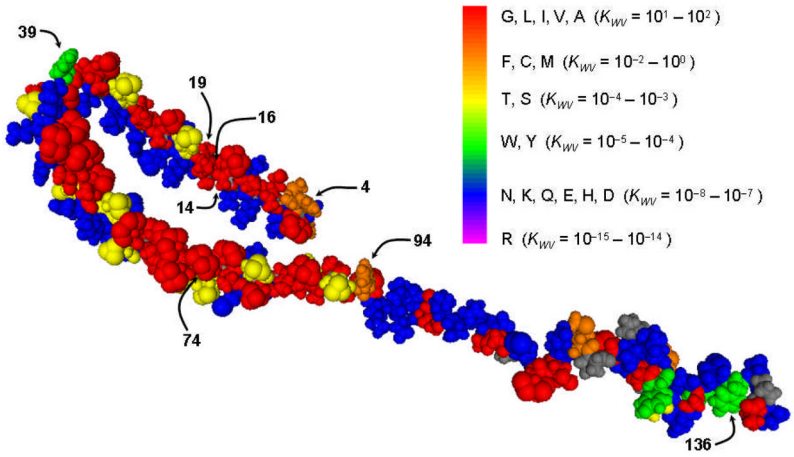

Figure 6.

Model of the structure of α-syn bound to micelles (Ref. 30) Amino acid sidechains are colored according to their equilibrium constants for transfer from water to vapor (Ref. 29): $1 < K_{WV} < 10^{2}$, G, L, I, V, A (red); $10^{-2} < K_{WV} < 1$, F, C, M (orange); $10^{-4} < K_{WV} < 10^{-3}$, T, S (yellow); $10^{-5} < K_{WV} < 10^{-4}$, W, Y (green); $10^{-8} < K_{WV} < 10^{-7}$, N, K, Q, E, H, D (blue); $10^{-15} < K_{WV} < 10^{-14}$, R (magenta). K_{WV} was not reported for a P sidechain analogue; these residues are shown in grey. Locations of donor/acceptor sites for contact rate measurements (Table 4) are indicated.

TABLE 1

Analytical and Monte Carlo Calculations of Mean Walklengths ($\langle x \rangle$) for Synchronous and Asynchronous Motion on One-Dimensional Periodic Lattices

	Asynchronous $\langle x \rangle$			Synchronous $\langle x \rangle$		
sites (N)	Analytical[a]	Monte Carlo	error	Analytical[b]	Monte Carlo	error
3	2.000	1.999	0.050%	2.000	1.999	0.050%
4	3.333	3.334	0.020%	3.333	3.335	0.050%
5	5.000	5.001	0.020%	4.000	4.000	0.000%
6	7.000	7.004	0.057%	5.600	5.603	0.054%
7	9.333	9.330	0.036%	6.667	6.665	0.025%
8	12.000	11.993	0.058%	8.571	8.565	0.075%
9	15.000	15.011	0.073%	10.000	10.008	0.080%
10	18.333	18.343	0.053%	12.222	12.232	0.080%
11	22.000	22.016	0.073%	14.000	14.005	0.036%
12	26.000	25.978	0.085%	16.545	16.525	0.124%
13	30.333	30.327	0.021%	18.667	18.647	0.105%
14	35.000	34.967	0.094%	21.538	21.551	0.058%
15	40.000	40.025	0.062%	24.000	23.999	0.004%
16	45.333	45.364	0.068%	27.200	27.196	0.015%
17	51.000	50.987	0.025%	30.000	30.034	0.113%
18	57.000	56.913	0.153%	33.529	33.531	0.005%
19	63.333	63.365	0.050%	36.667	36.664	0.007%
20	70.000	70.011	0.016%	40.526	40.533	0.016%

[a] Ref. 15–17

[b] Ref. 14

Table 2

Asynchronous and Synchronous Mean Walklengths ($\langle x \rangle$) on Three-Dimensional Cubic Lattices with Maximum Loop

			Asynchronous $\langle x \rangle$			Synchronous $\langle x \rangle$	
Loop (*n*)	**Lattice**	**Sites (*N*)**	**Markov result**	**Monte Carlo estimate**	**%error**	**Monte Carlo estimate**	**95% confidence interval of the mean**
6	2×2×2	8	16.571	16.532	0.235%	10.055	0.101
8	2×2×3	12	29.376	29.459	0.283%	15.833	0.158
10	3×3×2	18	47.130	47.289	0.337%	24.071	0.241
12	3×3×3	27	72.274	72.365	0.126%	34.817	0.348
14	3×3×4	36	102.855	103.035	0.175%	47.307	0.473
18	4×4×4	64	194.586	193.547	0.534%	84.192	0.842
24	5×5×5	125	409.609	412.004	0.585%	164.209	1.642
30	6×6×6	216	743.332	749.157	0.784%	280.770	2.808
36	7×7×7	343	1221.708	1233.597	0.973%	448.451	4.484

Table 3

Monte Carlo Estimates of Synchronous and Asynchronous Mean Walklengths ($\langle x \rangle$) on a 3D Cubic Lattice with Chain Extension

		Asynchronous (p = 0)		Synchronous (p = 1)	
chain length (n)	**Spherical shell sites [a]**	$\langle x \rangle$	**95% confidence interval of the mean**	$\langle x \rangle$	**95% confidence interval of the mean**
6	925	1298.372	64.897	1103.828	55.148
8	2109	2954.236	28.844	2480.986	124.001
10	4169	5928.55	57.619	4984.218	249.177
12	7153	10194.093	99.257	8547.045	426.992
14	11513	16604.537	830.193	14214.112	710.401
18	24405	35628.469	1780.921	30200.068	1509.801
24	57777	88177.585	4406.713	71158.106	3557.090
30	113081	182277.017	9109.618	148688.928	7434.165
36	195269	300444.344	15008.916	240790.980	12031.165

[a] The number of sites on a cubic lattice that fall within a spherical shell of radius r equal to the chain length (n).

Table 4

Average α-syn Contact Rate Constants and Mass Ratios

loop size (*n*)	W site	Y(NO_2) site	$\langle k \rangle$, s^{-1}	*R*
10	4	14	5.1×10^6	0.031
12	4	16	2.3×10^6	0.032
15	4	19	7.2×10^5	0.033
20	94	74	2.8×10^5	0.704
20	39	19	2.6×10^5	0.179
35	4	39	5.3×10^5	0.039
42	94	136	2.3×10^5	0.046
55	94	39	1.6×10^5	0.747
90	4	94	2.2×10^5	0.079
132	4	136	3.9×10^5	0.960